Spatially informed phenotyping by cyclic-in-situ-hybridisation identifies novel fibroblast populations and their pathogenic niches in systemic sclerosis

Yi-Nan Li, Tim Filla, Andrea-Hermina Györfi, Minrui Liang, Veda Devakumar, Alexandru Micu, Hongtao Chai, Christina Bergmann, Ann-Christin Pecher, Jörg Henes, Pia Moinzadeh, Suzan Al-Gburi, Thomas Krieg, Alexander Kreuter, Jiucun Wang, Georg Schett, Bernhard Homey, Sascha Dietrich, Jörg H.W. Distler, Alexandru-Emil Matei

Article - Version of Record

Ann Rheum Dis 84 (2025) 1852–1864

Contents lists available at ScienceDirect

Annals of the Rheumatic Diseases

journal homepage: https://www.sciencedirect.com/journal/annals-of-the-rheumatic-diseases

Systemic sclerosis

Spatially informed phenotyping by cyclic-in-situ-hybridisation identifies novel fibroblast populations and their pathogenic niches in systemic sclerosis

Yi-Nan Li[1,2,*], Tim Filla[1,2], Andrea-Hermina Györfi[1,2,3], Minrui Liang[1,2,4], Veda Devakumar[1,2], Alexandru Micu[1,2], Hongtao Chai[1,2], Christina Bergmann[5,6], Ann-Christin Pecher[7], Jörg Henes[7], Pia Moinzadeh[8], Suzan Al-Gburi[8], Thomas Krieg[9,10,11], Alexander Kreuter[12], Jiucun Wang[4,13,14], Georg Schett[5,6], Bernhard Homey[15], Sascha Dietrich[16], Jörg H.W. Distler[1,2,3,*], Alexandru-Emil Matei[1,2,3,*]

[1] *Department of Rheumatology, University Hospital Düsseldorf, Heinrich Heine University, Düsseldorf, Germany*
[2] *Hiller Research Center, University Hospital Düsseldorf, Heinrich Heine University, Düsseldorf, Germany*
[3] *Fraunhofer Institute for Translational Medicine and Pharmacology ITMP, and Fraunhofer Cluster of Excellence for Immune Mediated Diseases CIMD, Frankfurt am Main, Germany*
[4] *Department of Rheumatology, Huashan Hospital, Fudan University, Shanghai, P. R. China*
[5] *Department of Internal Medicine 3, Rheumatology and Clinical Immunology, Friedrich-Alexander-University Erlangen-Nürnberg (FAU) and University Hospital Erlangen, Erlangen, Germany*
[6] *Deutsches Zentrum Immuntherapie (DZI), FAU Erlangen-Nürnberg and University Hospital Erlangen, Erlangen, Germany*
[7] *Department of Internal Medicine II, Hematology, Oncology, Clinical Immunology, and Rheumatology, University Hospital Tübingen, Tübingen, Germany*
[8] *Department of Dermatology, University Hospital Cologne, Cologne, Germany*
[9] *Center for Molecular Medicine Cologne (CMMC), University of Cologne, Cologne, Germany*
[10] *Translational Matrix Biology, Faculty of Medicine, University Hospital Cologne, Cologne, Germany*
[11] *Cologne Excellence Cluster on Cellular Stress Responses in Ageing-Associated Diseases (CECAD), University of Cologne, 50931, Cologne, Germany*
[12] *Department of Dermatology, Venereology and Allergology, Helios St. Elisabeth Klinik Oberhausen, Duisburg, Germany*
[13] *State Key Laboratory of Genetic Engineering, Collaborative Innovation Center for Genetics and Development, School of Life Sciences, and Human Phenome Institute, Fudan University, Shanghai, P. R. China*
[14] *Research Unit of Dissecting the Population Genetics and Developing New Technologies for Treatment and Prevention of Skin Phenotypes and Dermatological Diseases (2019RU058), Chinese Academy of Medical Sciences, Shanghai, P. R. China*
[15] *Department of Dermatology, University Hospital Düsseldorf, Heinrich Heine University, Düsseldorf, Germany*
[16] *Department of Hematology, Oncology and Clinical Immunology, University Hospital Düsseldorf, Heinrich Heine University, Düsseldorf, Germany*

*Correspondence to** Prof. Jörg H.W. Distler, Dr. Alexandru-Emil Matei and Dr. Yi-Nan Li, Department of Rheumatology and Hiller Research Center, University Hospital Düsseldorf, Heinrich Heine University Düsseldorf, Düsseldorf, Germany.

E-mail addresses: yi-nan.li@med.uni-duesseldorf.de (Y.-N. Li), joerg.distler@med.uni-duesseldorf.de (J.H.W. Distler), Alexandru-Emil.Matei@med.uni-duesseldorf.de (A.-E. Matei).

Yi-Nan Li, Jörg H W Distler, and Alexandru-Emil Matei contributed equally.

Handling editor Josef S. Smolen.

https://doi.org/10.1016/j.ard.2025.06.002

ARTICLE INFO

Article history:
Received 10 January 2025
Received in revised form 30 May 2025
Accepted 1 June 2025

ABSTRACT

Objectives: Spatially nonresolved transcriptomic data identified several functionally distinct populations of fibroblasts in health and disease. However, in-depth transcriptional profiling *in situ* at the single-cell resolution has not been possible so far. We thus aimed to profile these populations by single-cell spatial transcriptomics using cyclic in situ hybridisation (cISH).

Methods: We studied fibroblast subpopulations in the skin of systemic sclerosis (SSc) patients and heathy individuals using cISH as a novel approach for transcriptional phenotyping with subcellular resolution. Clustering was performed using Building Aggregates with a Neighbourhood Kernel and Spatial Yardstick (BANKSY) as a novel approach for spatially informed transcriptional phenotyping. The findings were further validated by integration with single-cell RNA sequencing in distinct SSc cohorts.

Results: BANKSY-based spatially informed clustering identified 9 fibroblast (FB) subpopulations, with SFRP2+ reticular dermis (RetD) FB and CCL19+ nonperivascular (nonPV) FBs as novel subpopulations that reside in specific cellular niches and display unique gene expression profiles. SFRP2+ RetD FBs and CCL19+ nonPV FBs as well as COL8A1+ FBs display altered frequencies in SSc skin and play specific, disease-promoting roles for extracellular matrix release and leukocyte recruitment as revealed by their transcriptional profile, their cellular interactions, and ligand–receptor analyses. The frequencies of COL8A1+ FBs and their interactions with monocytic cells and B cells are associated with the progression of skin fibrosis in SSc.

Conclusions: Our cISH-based, spatially resolved transcriptomic approach identified novel fibroblast subpopulations deregulated in SSc skin with specific pathogenic roles. COL8A1+ FBs and their immune interactions may also have potential as biomarkers for future progression of skin fibrosis.

WHAT IS ALREADY KNOWN ON THIS TOPIC

- Single-cell RNA sequencing studies revealed that fibroblasts are a heterogenous population of cells with functionally diverse subpopulations. However, these studies lack spatial context and did not enable characterisation of the local niches and the cellular interactions *in situ*.

WHAT THIS STUDY ADDS

- We provide the first cyclic *in situ* hybridisation (cISH)-based characterisation of fibroblast subpopulations and their microenvironment in systemic sclerosis (SSc) and control skin.
- Using cISH in conjunction with a novel clustering approach that considers spatial localisation, we identify 9 subpopulations of fibroblasts, with recovery of previously described populations and identification of several novel subpopulations of fibroblasts.
- SFRP2+ reticular dermis (RetD), CCL19+ nonperivascular (nonPV), and COL8A1+ fibroblasts are numerically altered in SSc, reside in specific niches, and display unique cellular functions in SSc.
- SFRP2+ RetD, CCL19+ nonPV, and COL8A1+ fibroblasts display specific profibrotic, proinflammatory or dual profibrotic and proinflammatory roles in SSc skin.
- The frequencies of COL8A1+ fibroblasts and their interactions with monocytic cells or B cells are associated with progression of skin fibrosis.

HOW THIS STUDY MIGHT AFFECT RESEARCH, PRACTICE OR POLICY

- The newly identified fibroblast subpopulations may offer potential for selective targeting of SFRP2+ RetD, CCL19+ perivascular, and COL8A1+ fibroblasts as disease-promoting fibroblast subsets.
- COL8A1+ fibroblast counts and cellular interactions may offer potential as biomarkers for progression of skin fibrosis in SSc.

INTRODUCTION

Systemic sclerosis (SSc) is a connective disease characterised by autoimmunity and inflammation, which promote extensive fibrotic remodelling of the skin and various internal organs [1]. The progressive accumulation of the extracellular matrix (ECM) in affected tissues impairs organ function and commonly leads to organ failure, resulting in high morbidity and mortality of SSc patients [2]. Fibroblasts are the key effector cells for release of the ECM in fibrosis [2–5]. However, fibroblasts are a heterogenous population of cells with specific, functionally distinct subpopulations. Understanding fibroblast heterogeneity, particularly in the context of specific diseases, is still in its early stages. Moreover, we are lacking information on the organisation of fibroblast subpopulations *in vivo* and the intricate cellular interactions that occur within their native tissue environment.

Single-cell omics allows for the study of cellular subpopulations at previously unattainable resolution. To date, nonspatially resolved single-cell RNA sequencing (scRNA-seq) has been predominantly used to phenotype cellular changes in rheumatic diseases. scRNA-seq revealed that fibroblasts constitute a heterogenous population of cells with distinct transcriptional patterns and functions [6]. scRNA-seq data from SSc skin revealed between 6 and 10 distinct subpopulations of fibroblasts [7–9]. However, scRNA-seq, like other existing single cell techniques, requires tissue disaggregation and single cell separation. As a result, these approaches cannot provide information on the spatial localisation of cells inside the tissue, and they cannot characterise tissue niches and the cellular interplay that occurs within them. Spatial sequencing approaches overcome the lack of spatial context, but approaches published so far have a modest resolution of around 100 µm and are thus not able to resolve individual cells [7]. Here, we aimed to overcome these limitations using cyclic *in situ* hybridisation as a spatial transcriptomic approach with subcellular resolution of 120 nm.

METHODS

Patient and public involvement

Patients and/or the public were not involved in the design, conduct, reporting, or dissemination plans of our study.

Statistics

Data are presented as dot plots with the median ± IQR. Each dot represents one biological replicate, unless indicated otherwise in the figure legend. Protein expression levels are shown as heatmaps representing the mean of the Z score-normalised values. GraphPad Prism 8 was used to generate dot plots and to perform statistical analyses. Heatmaps were generated using the imcRtools R package [10]. Mann–Whitney *U* tests were applied for the comparison between 2 groups, if not indicated otherwise. Sensitivity analyses of fibroblast population frequencies were conducted using beta regression models with sex and age included as covariates using the betareg R package. Statistical analysis of activity scores was performed by linear mixed modelling fitted with donor-specific random intercepts using lmerTest R package. The comparison between SSc and controls was based on the estimated marginal means obtained from the linear mixed model using the emmeans R package.

RESULTS

Study design and identification of major cell types in SSc and control skin by cISH

We performed cISH from skin samples of SSc patients enriched for early, diffuse cutaneous involvement, with clinically active disease and sex-matched and age-matched healthy controls (Fig 1A; Supplementary Tables S1, S2, and Figure S1). We recovered a total of 20,979 cells (patients with SSc: 9876 cells; healthy individuals: 11,103 cells) (Fig 1A-C). These single cells included 3764 fibroblasts, identified by their high expression levels of *COL1A1, COL1A2, COL3A1*, and *DCN* (Fig 1B,D). We further identified other major cell populations from human skin, including keratinocytes (expressing *KRT1, KRT10, KRT14*, and *KRT15*), immune cells (expressing the panleukocyte gene *PTPRC* and specific genes for immune cells from the lymphoid and myeloid lineages such as *CD4, CD68, CD163*, and *LYZ*), endothelial cells (expressing *PECAM1, CDH5, ENG,* and *VWF*), and vascular smooth muscle cells (expressing *TAGLN, ACTA2,* and *MYL9*) (Fig 1D). These cell types had the expected spatial distribution in human skin, further validating their identity (Fig 1E).

Spatially informed phenotyping of fibroblasts in SSc and control skin identifies new fibroblast subpopulations

Using Building Aggregates with a Neighbourhood Kernel and Spatial Yardstick (BANKSY) as an algorithm that leverages the spatial information to perform clustering based not only on the own gene expression, but also on the average expression and expression gradients among each cell's neighbours [11], we identified 9 subpopulations of fibroblasts and annotated them based on their differential marker expression and on the spatial localisation. In accordance with previous studies [6–9], we identified COL8A1+ FBs, PI16+ FBs, ACKR3+ FBs, GSN+ FBs, and DUSP+ FBs, thus confirming the validity of this approach (Fig 2).

In addition, BANKSY-based clustering identified novel subpopulations that were not resolved using nonspatial approaches (Supplementary Fig S2). Two of the BANKSY-based clusters corresponded to the SFRP2+ FBs as defined by nonspatial clustering (Supplementary Fig S3A-C). In addition, 1 of the 2 SFRP2+ populations was located in spatial proximity to the epidermal layer and was thus termed SFRP2+ papillary dermis (PapD) FB. The other SFRP2+ population was located deeper in the dermis and was thus termed SFRP2+ reticular dermis (RetD) FB (Supplementary Fig S3D). The average expression and expression gradients of the keratinocyte markers *KRT14* and *KRT5* were higher among the neighbouring cells of SFRP2+ FB RetD than those of the SFRP2+ FB PapD (Supplementary Fig S3F), further confirming their distinct spatial distribution.

BANKSY-based clustering also identified 2 subpopulations of the previously described CCL19+ FB cluster as defined by nonspatial clustering (Supplementary Fig S3A-C). One of the CCL19+ FB clusters that we termed CCL19+ perivascular (PV) FBs was located around endothelial cells and consistently had a higher expression of the endothelial cell marker *PECAM1* and the pericyte marker *RGS5* among its neighbours than the CCL19+ nonperivascular (nonPV) FBs (Supplementary Fig S3E, G). The latter subpopulation was diffusely distributed in the dermis without enrichment in a particular dermal compartment (Supplementary Fig S3E).

Of particular note, the SFRP2+ RetD and the CCL19 PV FBs are not only distinct from the SFRP2+ PapD and the CCL19 nonPV FBs, respectively, with regards to their spatial location, but also with regards to their own gene expression, demonstrating functional differences of these newly identified subpopulations. For example, SFRP2+ RetD expressed higher levels of *COL1A1* and *COL3A1* than SFRP2+ PapD FBs. CCL19+ nonPV expressed higher levels of *CXCL12* and *PTGDS* than the CCL19+ PV FBs (Fig 2D).

In contrast, the other 5 subpopulations of fibroblasts defined by nonspatial clustering were homogenous not only regarding their own gene expression, but also to their spatial distribution (Fig 2D, Supplementary Fig S3A-C).

Integration with 2 scRNA-seq datasets, i.e. GSE138669 [6] and GSE195452 [8], demonstrated that neither of the label transfer-based annotations from the scRNA-seq to the cISH dataset could reliably distinguish between the SFRP2+ PapD and RetD FBs or between the CCL19+ PapD and RetD FBs, respectively (Supplementary Figs S4, S5). This finding highlights that the spatially informed BANKSY-based annotation can refine the fibroblast phenotyping performed with previous methods.

Changes in frequencies of fibroblast subpopulations in SSc skin

SFRP2+ RetD FBs and the COL8A1+ FBs had significantly higher frequencies in SSc, whereas PI16+ FBs, DUSP+ FBs, and CCL19+ PV FBs had modestly lower frequencies in SSc (Fig 3). These changes in the frequencies of COL8A1+ FBs and PI16+ FBs are consistent with those reported by scRNA-seq-based studies [6–9]. Of note, the populations resolved only by BANKSY clustering demonstrated distinct changes in SSc. SFRP2+ PapD FBs were numerically decreased in frequency in SSc, whereas SFRP2+ RetD FBs were increased. In addition, CCL19+ nonPV FBs were numerically increased in SSc, whereas CCL19+ PVs were decreased (Fig 3A,C,E). As cell composition may be influenced by donor sex and age, we performed a sensitivity analysis including these variables as covariates. This analysis excluded those variables as major confounders for the frequencies of fibroblasts in SSc (Supplementary Table S3).

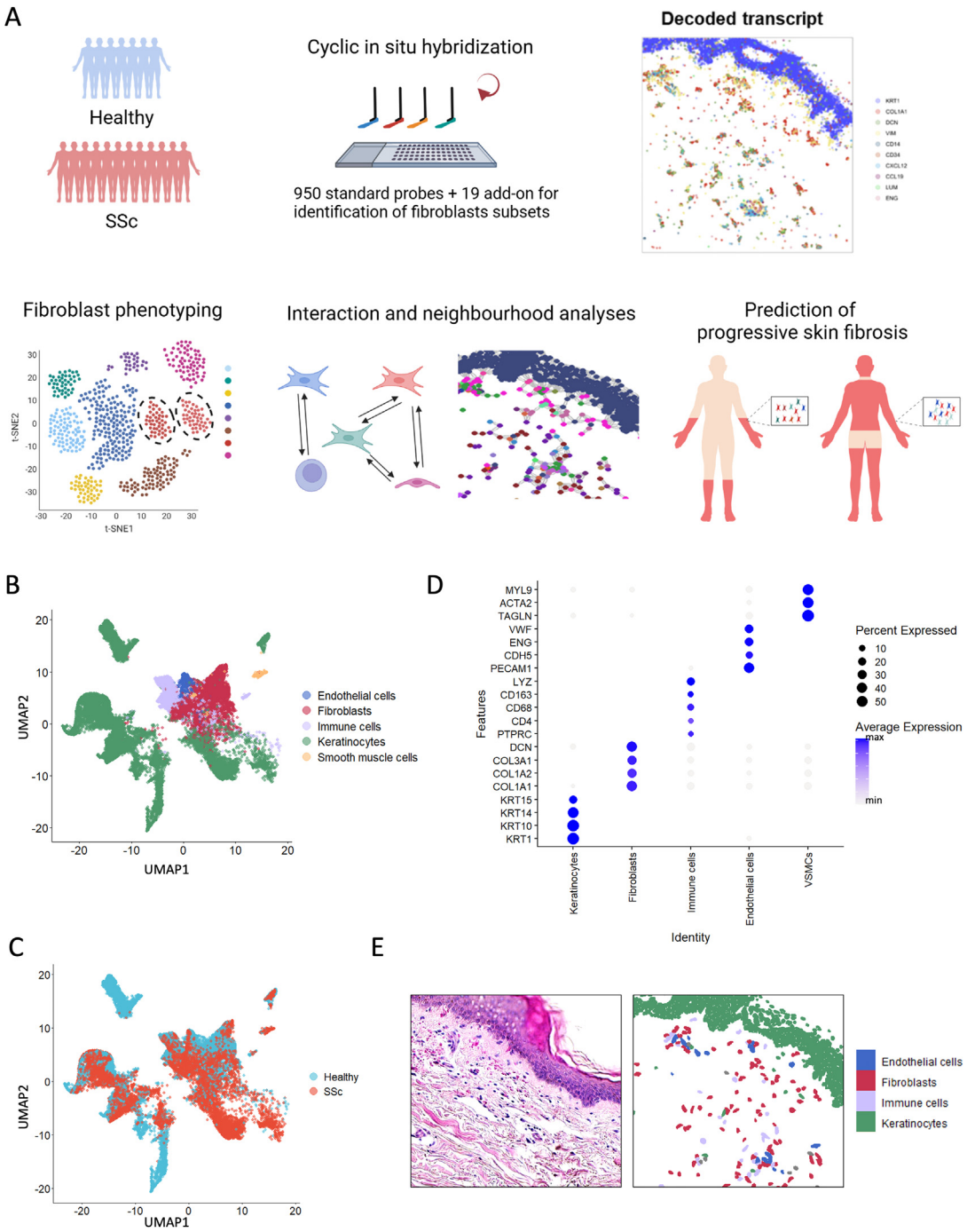

Figure 1. Characterisation of skin tissue organisation in SSc using cISH. A, Schematic overview of the experimental and analytic workflow. The transcriptomic profiles of skin tissue from healthy and SSc donors were analysed with imaging-based spatial transcriptomics using cISH. The cell populations in the skin were characterised based on the transcriptional profile. Taking advantage of spatial information, we performed cellular interaction analysis and evaluated whether changes in cell frequencies or spatial relationships might predict progression of skin fibrosis. B, UMAP plot showing 20,979 cells detected in the skin samples. The plot is coloured by the major cell types within the skin tissue. C, UMAP plot showing the cells detected in the skin samples obtained from healthy donors and SSc patients. D, Dot plot indicating marker gene expression of the major cell populations in the skin tissue. The size of the dot represents the percentage of the cells that expressed the specified gene. The dots were coloured by levels of the expression of specified gene. E, Representative images of HE staining and distribution of cISH-detected cells in the skin tissue. This figure was created with BioRender.com. cISH, cyclic *in situ* hybridisation; HE, haematoxylin and eosin; SSc, systemic sclerosis; UMAP, uniform manifold approximation and projection.

We next performed pseudotime analysis on the spatially informed fibroblast subsets using Monocle [12]. We defined PI16+ FBs as the root (starting point) of the pseudotime because they were previously described as a fibroblast subset with stem cell properties that can differentiate into specialised fibroblasts [13,14]. The pseudotime analysis revealed 3 differentiation trajectories: one trajectory going through SFRP2+ PapD FBs and ending with DUSP+ FBs; one trajectory going through CCL19+ PV FBs, then through CCL19+ nonPV FBs, and ending with GSN+ FBs; and a third trajectory going through ACKR3+ FBs, followed by SFRP2+ RetD FBs, and ending with COL8A1+ FBs (Supplementary Fig S6). The latter differentiation trajectory started from a fibroblast subset with decreased frequency in SSc and ended with 2 subsets that are highly enriched in SSc. This suggests that the fibroblast subsets enriched in SSc are terminally differentiated from precursor fibroblasts (among

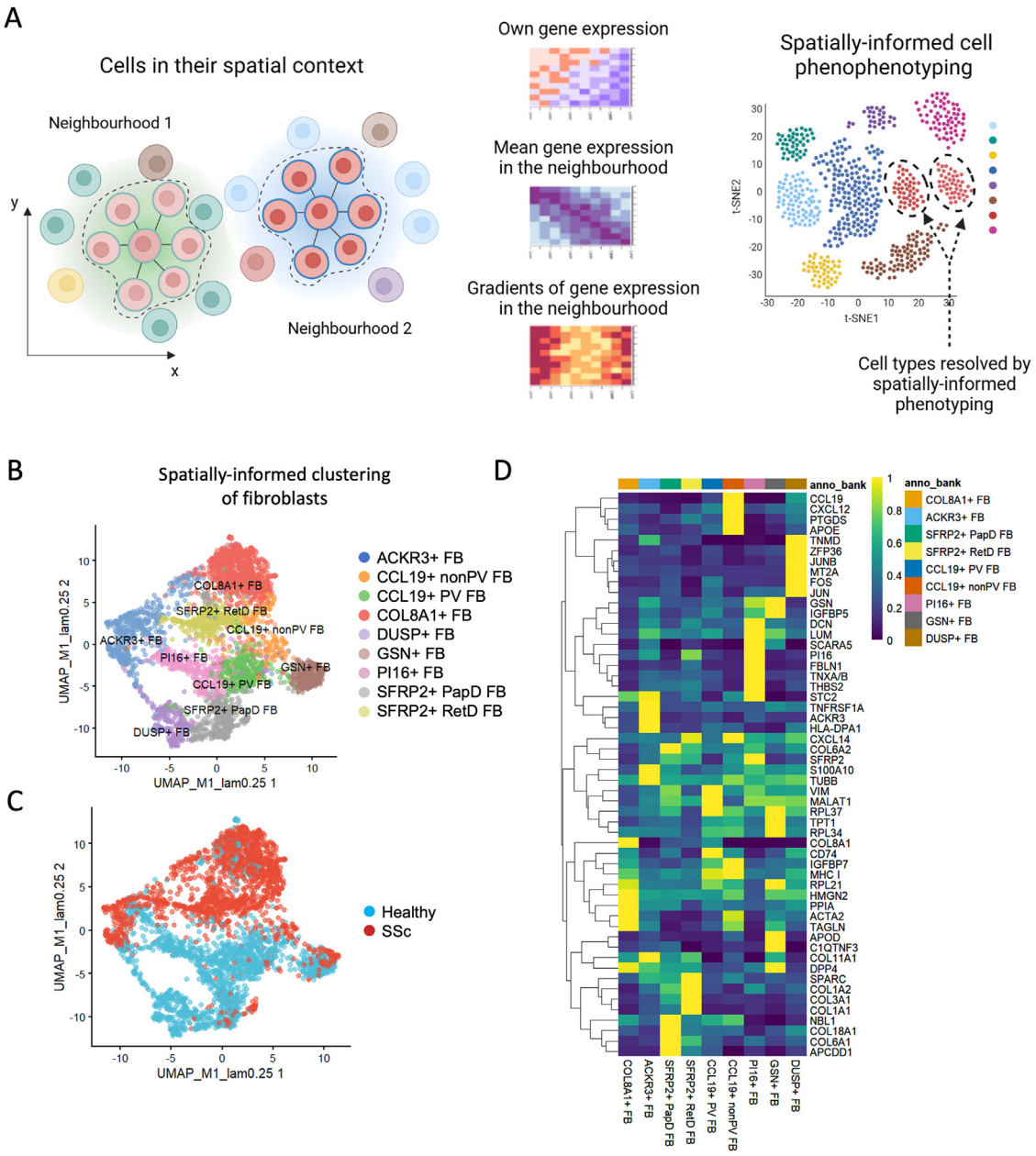

Figure 2. Fibroblasts populations identified by spatially informed clustering. A, An illustration showing the workflow for spatially informed cell phenotyping using BANKSY-based spatial clustering. In addition to the expression matrix of the cell of interest, the transcriptional profiles of the local environment, including averaged expression and the expression gradient of neighbouring cells, were computed using BANKSY and subjected to phenotyping by clustering. B, UMAP showing fibroblast populations identified by spatially informed clustering using BANKSY. C, UMAP showing the BANSY-identified populations from healthy and SSc donors. D, Expression heatmap of the marker genes for the BANKSY-identified populations. This figure was created with BioRender.com. BANKSY, Building Aggregates with a Neighbourhood Kernel and Spatial Yardstick; SSc, systemic sclerosis; UMAP, uniform manifold approximation and projection.

other cell types), in line with previous publications [13–15]. Of note, while the CCL19+ PV FB and CCL19+ nonPV FB subsets aligned along one trajectory and are thus likely developmentally related, the SFRP2+ PapD FB and the SFRP2+ RetD FB subsets were located along 2 distinct trajectories.

Functional heterogeneity of the spatially informed fibroblast subsets

We next aimed to further characterise the functional of spatially resolved subpopulations. We first computed an ECM module score, as well as scores for different ECM components with the gene sets curated in the Matrisome project (Fig 4A, Supplementary S7A) [16]. The SFRP2+ RetD FB subpopulation had the highest ECM score and collagen score of all fibroblast subpopulations (Fig 4A), while the PI16+ FBs had the highest glycoproteins and proteoglycans scores (Supplementary Fig S7A), pointing to specific roles in ECM production for the different subsets. Transforming growth factor (TGF) β pathway activity inferred using Pathway Responsive Genes for Activity Inference signatures [17] was most enriched in SFRP2+ RetD FBs (Supplementary Fig S7B). Comparison of fibroblast populations in SSc and normal skin revealed higher ECM and collagen scores and TGFβ activity for several fibroblast populations in SSc skin, including in SFRP2+ PapD FBs and CCL19+ nonPV FBs (Supplementary Fig S7C).

To validate these findings, we performed 2 complementary computational approaches. We first applied the algorithm CytoSPACE [18] to map to the cISH dataset 2 publicly available scRNA-seq datasets of SSc and healthy skin (GSE195452 and

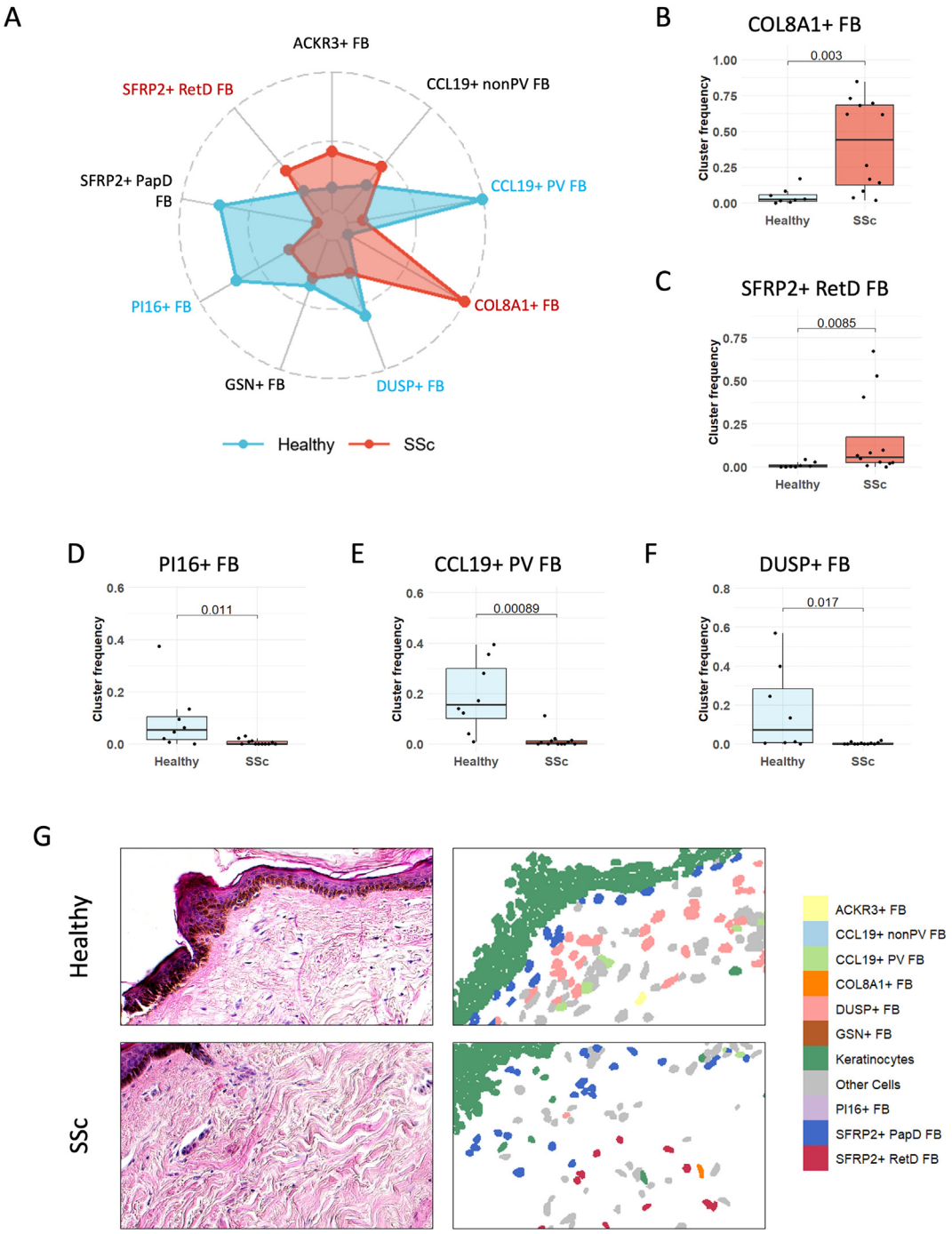

Figure 3. Changes in frequencies of fibroblast subsets identified by spatially informed phenotyping in SSc. A, An overview of the changes in the abundance of BANKSY-identified fibroblast populations. The abundance was quantified by the proportion of the specified population within the fibroblast component. Z score-normalised median proportions were plotted on the radar chart. The statistically significant changes were highlighted in red (increased in SSc) and blue (increased in healthy). B-F, Changes in frequencies of COL8A1+ FB (B), SFRP2+ RetD FB (C), PI16+ FB (D), CCL19+ PV FB (E), and DUSP+ FB (F) in SSc compared to control skin. G, Representative images of BANKSY-identified populations in the skin tissue, along with HE stainings of the corresponding regions. The statistical significance was determined by the Mann–Whitney *U* test. *P* values below 0.05 were considered significant. BANKSY, Building Aggregates with a Neighbourhood Kernel and Spatial Yardstick; HE, haematoxylin and eosin; SSc, systemic sclerosis.

GSE249279 [7,8]). The ECM and collagens scores as well as the TGFβ pathway activity computed from the enhanced cISH dataset were enriched in SFRP2+ RetD FBs (Supplementary Fig S8A), whereas the glycoproteins and proteoglycans scores were enriched in PI16+ FBs (Supplementary Fig S8B).

We next performed functional enrichment analysis using the fast gene set enrichment analysis and the univariate linear model (ULM) methods via decoupleR [19]. Both methods revealed that the fibroblast subsets have both shared and distinct biological functions (Fig 4B, Supplementary Fig S9A). The SFRP2+ RetD FBs are profibrotic, ECM-producing fibroblasts. They demonstrated the highest enrichment scores for pathways related to fibrosis, such as 'collagen formation', 'response to TGFβ', and 'positive regulation of WNT signalling pathway' (Fig 4B, Supplementary Fig S9A). In contrast, 'response to mechanical stimulus' was specifically enriched in SFRP2+ RetD FBs (Supplementary Fig S9A). SFRP2+ PapD FBs demonstrated enriched pathways specific for this population, i.

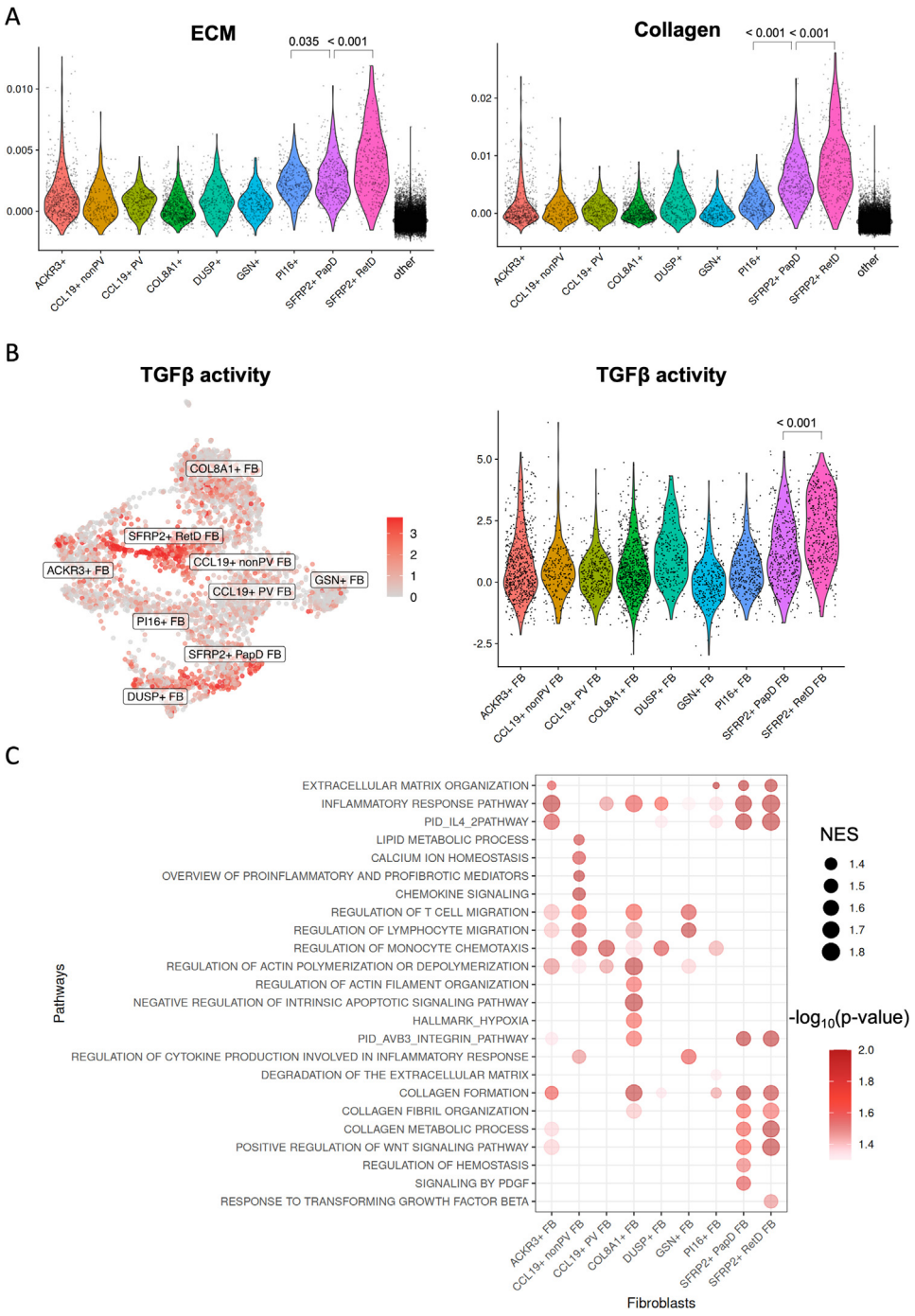

Figure 4. Distinct biological functions of spatially identified fibroblast populations. A, Violin plots showing the ECM module scores of components obtained from the Matrisome project across fibroblast populations detected in SSc and control skin. Nonfibroblast populations were labelled as 'other' in the violin plots. B, UMAP and violin plots illustrating TGFβ activities inferred using PROGENy signatures across fibroblast populations. C, Dot plot showing the pathway enrichment scores across fibroblasts populations computed by FGSEA for pathways with a P value < .05. The pathway enrichment analysis was performed using decoupleR R package using the pseudo-bulk expression matrix that contained averaged expression for each fibroblast subpopulation. Statistical significance was assessed by comparing estimated marginal means from linear mixed models including donor-specific random intercepts. P values are shown above each comparison. ECM, extracellular matrix; FGSEA, fast gene set enrichment analysis; NES, normalised enrichment score; PROGENy, Pathway Responsive Genes for Activity Inference; TGFβ, tumour growth factor β; UMAP, uniform manifold approximation and projection.

e. 'signalling by platelet-derived growth factor (PDGF)', and de-enriched for 'immune response' (Fig 4B and Supplementary Fig S9A). CCL19+ nonPV FBs are an inflammatory fibroblast population. Shared functions of CCL19+ PV and nonPV FBs included several terms related to cytokine production and immune responses. Specific functions of CCL19+ PV FB included a high enrichment score on 'regulation of monocyte chemotaxis' and de-enrichment of 'immune system process' compared to the enrichment of 'calcium ion homeostasis' and 'lipid metabolic process' in CCL19+ nonPV FBs (Fig 4B, Supplementary Fig S9A). These differences highlight that the fibroblasts populations separated by BANKSY clustering are not only distinct with regards to their spatial location in their differentiation trajectories, but also with regards to their function.

The COL8A1+ FBs may have broad spectrum of roles in modulating fibrotic and inflammatory responses as

demonstrated enrichment in pathways related to collagen organisation, but also in pathways such as 'regulation of lymphocyte migration' and 'regulation of monocyte chemotaxis' (Fig 4B, Supplementary Fig S9A). Furthermore, COL8A1+ FBs demonstrated specific enrichment of 'negative regulation of apoptotic signalling pathway', suggesting resistance to apoptosis. Of note, we detected stronger activity of terms related to immune and fibrotic modulation in these fibroblast populations in SSc compared to healthy controls (Fig S7B, Supplementary Fig S9B).

Multicellular spatial domains in SSc skin

Given the profound effects of crosstalk with neighbouring cells on cellular phenotype and function, we next aimed to characterise the local microenvironment of individual subpopulations of fibroblasts. We first annotated immune subpopulations by label transfer, using the scRNA-seq dataset GSE195452 as a reference (Supplementary Fig S10).

Identification of multicellular spatial domains, or cellular neighbourhoods (CNs), by clustering cells based on the composition of their neighbouring cells yielded 14 CNs (Supplementary Fig S11). We annotated the CNs according to their composition, i.e. to the cell population with the highest relative frequency inside each CN. Some of these CNs recovered histologically defined domains of the skin, e.g. the epithelium in the epithelial CN or the vascular region in the endothelial CN (Supplementary Fig S11). Most of the other CNs were mainly defined by the predominant fibroblast population, e.g. CCL19 nonPV CN, COL8 CN, SFRP2 CN, PI16 CN or CCL19 PV CN. SFRP2+ PapD FBs but not SFRP2+ RetD FBs were enriched in the subepithelial CN, whereas the CCL19+ PV FBs but not the CCL19+ nonPV FBs were enriched in the endothelial CN, confirming the spatial segregation of these populations with a distinct method (Supplementary Fig S11).

The composition of several CNs were remarkably different in SSc compared to normal skin, with an enrichment of immune cell subsets in the CCL19 nonPV CN, COL8 CN, and SFRP2 CN and with a de-enrichment of immune cells in the PI16 CN and CCL19 PV CN (Fig 5A). Furthermore, PI16+ FB were enriched in COL8 CN and SFRP2 CN in SSc and thus in spatial proximity to SFRP2+ RetD and COL8A1+ FBs. This indirectly supports the hypothesis that PI16+ FBs can differentiate to profibrotic fibroblast subsets in SSc (Fig 5A).

We reasoned that the changes in the composition of CNs in SSc can lead to functional changes within the local niches. Indeed, functional enrichment analysis demonstrated that fibroblast-enriched CNs, such as CCL19 nonPV CN, CCL19 PV CN, SFRP2 CN, PI16 CN, or COL8 CN, are functionally distinct in SSc compared to normal skin with changes in disease-relevant pathway enrichment scores (Fig 5B). Changes in SSc included the enhanced antiapoptotic and antigen processing activities in the CCL19 nonPV CN and COL8 CN in SSc. Activation of lymphocyte-mediated killing, including CD8 TCR signalling and apoptosis, was detected in CCL19+ PV CN in SSc. The SFRP2 CN was present exclusively in SSc skin and exhibited the highest scores in pathways related to ECM remodelling among the fibroblast-enriched CNs. These findings support the concept that the CNs identified are functional units within the skin that undergo pathologic changes in SSc.

Cell–cell interaction and communication networks in SSc skin

We next aimed to unravel changes in cell–cell interaction networks. Pairwise interaction analysis revealed distinct cellular interaction networks in SSc skin (Fig 5C, Supplementary Fig S12). CCL19+ nonPV FBs demonstrated increased interactions with several immune cell subsets, whereas CCL19 PV FBs showed decreased interactions with mast cells, B cells, and plasma cells in SSc compared to normal skin (Fig 5C). COL8A1+ FBs transitioned from an immune-inert state, as shown by the lack of interactions or even avoidance of immune cells, to an immune-engaging state, interacting with macrophages, dendritic cells, natural killer (NK) cells, and plasma cells in SSc (Fig 5C). In SSc skin, SFRP2+ PapD FBs interacted with T cells, and SFRP2+ RetD FBs interacted with mast cells and NK cells. These interactions were not observed in normal skin (Supplementary Fig S12).

We further performed spatially informed cell–cell communication analysis using CellChat [20]. This analysis revealed profound changes in the patterns of ligand-receptor (L–R) interactions in SSc compared to control skin (Fig 6, Supplementary Figs S13, S14). SFRP2+ RetD FBs demonstrated L–R interactions with several other fibroblast subsets and with mast cells, NK cells, or dendritic cells in SSc, whereas in control skin they were only communicating with other SFRP2+ RetD FBs (Fig 6A). In contrast, the SFRP2+ PapD FBs lost communication with multiple cell types in SSc (Fig 6A). Of note, CellChat analysis without spatial distance constraints, which did not account for spatial information, did not resolve these differences between SSc and normal skin and showed comparable L–R interactions for both SFRP2+ FB subsets (Supplementary Fig S13A).

At the signalling level, SFRP2+ RetD FB in SSc demonstrated an increased relative strength for outgoing, but a decreased strength for incoming signals for collagen and fibronectin1 compared to normal skin, which may point towards a reduced capacity for ECM sensing in SSc (Fig 6B, Supplementary Fig S13B). Indeed, further analysis indicated decreased ECM signals received by CD44, a receptor with well-characterised roles in ECM sensing [21], on SFRP2+ RetD FBs compared to other fibroblast populations in SSc (Supplementary Fig S14A). Furthermore, the CCL19+ nonPV FBs demonstrated an increased relative strength for outgoing signals for CXCL12 in SSc, suggesting a higher chemotactic capacity (Fig 5C, Supplementary Fig S14B). PDGF signalling also demonstrate subpopulation-specific differences in SSc skin:fibroblast subsets with increased frequency in SSc. For example, SFRP2+ RetD and COL8A1+ FBs started to receive PDGF signals in SSc. In contrast, in control skin, only fibroblast subsets with lower frequencies in SSc, such as SFRP2+ PapD and CCL19+ PV FBs, received PDGF signals, indicating a switch from homeostatic to pro-fibrotic roles of PDGF signalling in SSc (Supplementary Fig S13C). Furthermore, PDGF signals were sent by endothelial cells in SSc and by monocytes/macrophages in control skin.

These spatially resolved analyses demonstrate major changes in signalling between distinct fibroblast subsets and other cells in SSc skin that could not be resolved in nonspatial datasets.

Predictors of progression of skin fibrosis in SSc

We investigated whether the frequencies of fibroblast subpopulations—either on their own or stratified by their interaction partners—at the time of biopsy could predict the progression of skin fibrosis at follow-up. Patients with progression of skin fibrosis at follow-up had a higher frequency of COL8A1+ FBs than those with stable skin fibrosis (Fig 7A). Other fibroblast populations were not significantly different between the 2 groups (Supplementary Fig S15). Furthermore, COL8A1+ FBs in close

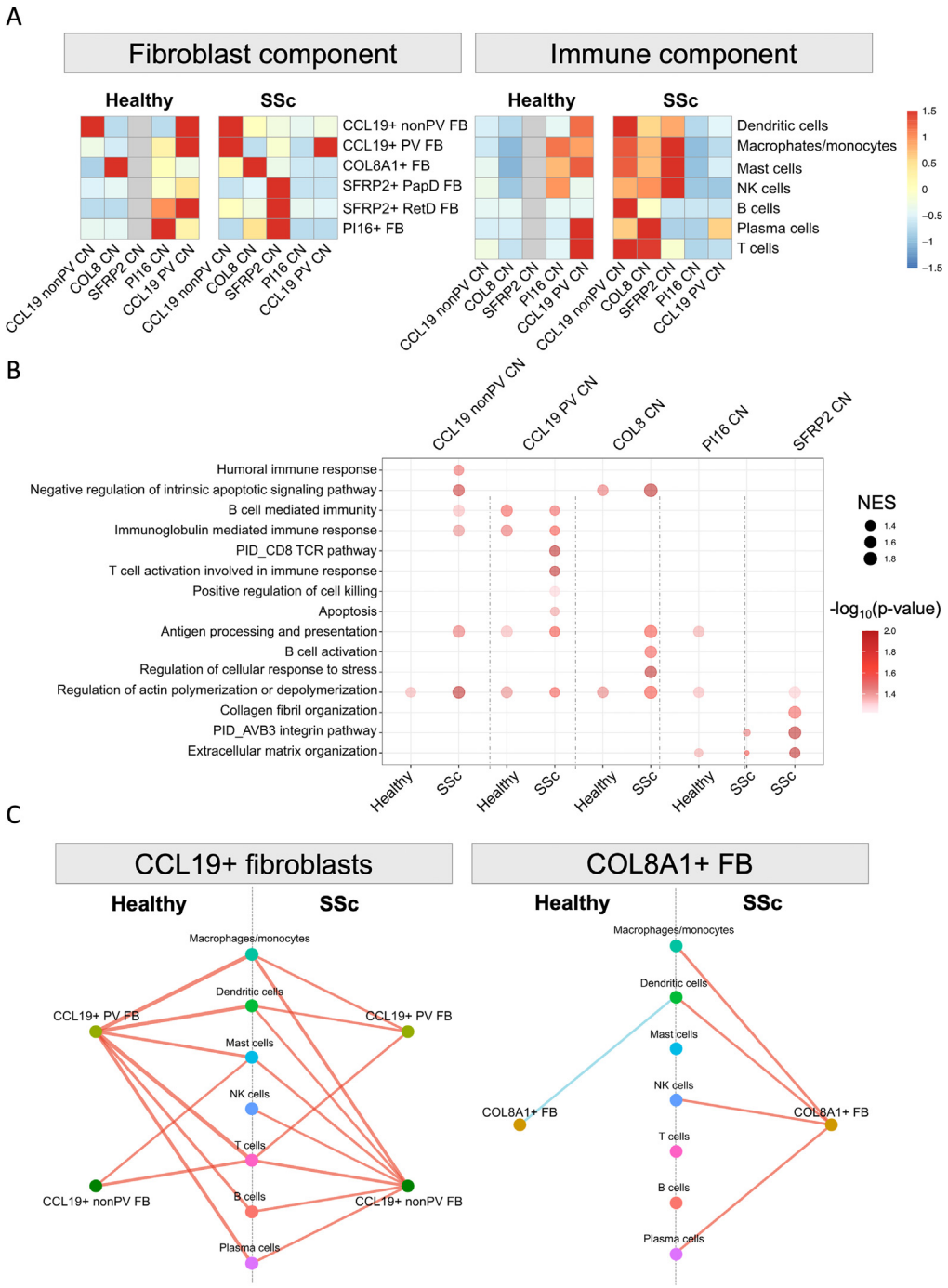

Figure 5. Changes in the cellular neighbourhoods in SSc skin. A, Heatmaps highlighting the shift in the cellular composition within the fibroblast CNs in healthy and SSc skin. The number of cells were normalised for each cell type across all CNs. SFRP2 CN was not detected in healthy samples and is shown in grey in the heatmap. B, Dot plot showing the activation of immuno- and matrix remodelling pathways within fibroblast CNs in SSc compared to healthy controls. The activation of the pathways was analysed by pseudo-bulk FGSEA. The size of the dot represents the NES, and the colour represents the *P* value. C, Network visualisation showing the immune interaction of indicated fibroblast populations in healthy and SSc skin by pairwise interaction analysis based on the cellular distribution in the tissue. Cellular attraction (red) and avoidance (blue) are indicated in the plots. The width of the lines represents the proportion of samples exhibiting statistically significant interaction. B-C, The statistical significance was determined by FGSEA (B) or using the permutation test (C). Results that did not reach statistical significance ($P < .05$) were excluded from the visualisations for clarity. CN, cellular neighbourhood; FGSEA, fast gene set enrichment analysis; NES, normalised enrichment score; SSc, systemic sclerosis.

spatial proximity to macrophages/monocytes, mast cells, or B cells had significantly higher frequencies in patients with progression of skin fibrosis, whereas COL8A1+ FBs with spatial proximity to other immune cell populations demonstrated only milder differences between the 2 groups (Fig 7B-D, Supplementary Fig S16A-D).

We further generated 2 least absolute shrinkage and selection operator predictive regression models with progression of skin fibrosis at follow-up as outcome. The first model that included the frequencies of the fibroblast subsets with shifts in frequencies in SSc skin as predictors for progression of skin fibrosis performed with a moderate accuracy and with an area under the curve (AUC) of 81% (Supplementary Fig S17). In a second model, we included the frequencies of COL8A1+ FBs with spatial proximity to macrophages/monocytes, mast cells, or B cells instead of the frequencies of all COL8A1+ FBs, while keeping

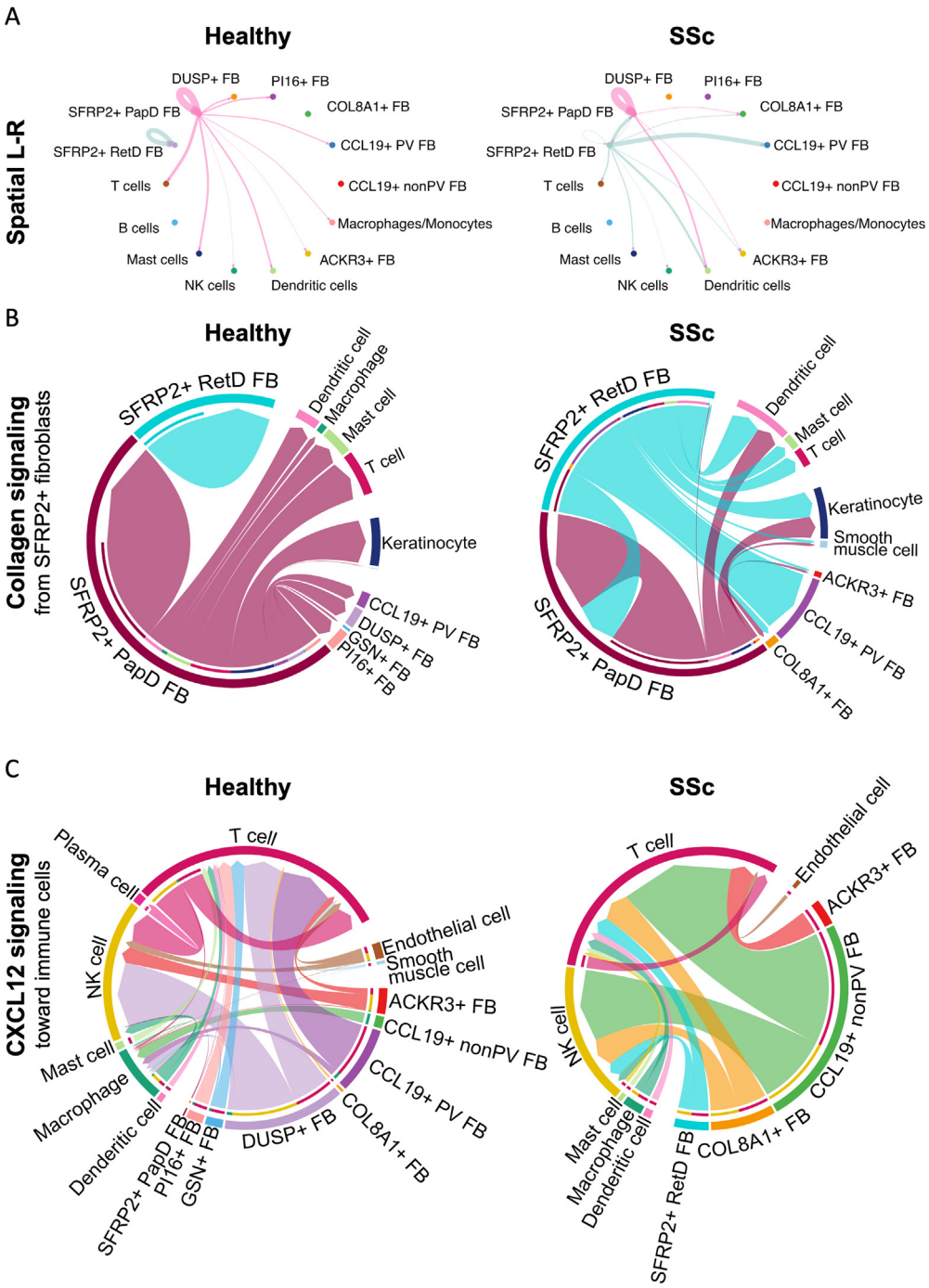

Figure 6. Distinct cell–cell communication in SSc identified by spatially informed ligand–receptor analysis. A, Representative circle plots showing the interaction of SFRP2-expressing fibroblasts in healthy and SSc skin by spatial ligand–receptor analysis using CellChat. The distance constraints were set to 250 μm for secreted signalling and 20 μm for contact-dependent signalling. Interaction routes are represented by lines, with line width indicating interaction strength as computed using CellChat. B, Chord diagrams showing the collagen signalling from the SFRP2-expressing fibroblasts. C, Chord diagrams showing the CXCL12 signalling received by immune cells and their source. In chord diagrams (B and C), the thinner inner bars represent the signalling strength received by the indicated targets. L–R, ligand–receptor analysis; SSc, systemic sclerosis.

the other predictors unchanged. This model demonstrated improved prediction accuracy, allowing a better separation between the predicted progressors and predicted stable patients, with an AUC of 95% (Fig 7E-H). The frequency of COL8A1+ in proximity to monocytes/macrophages was the most important feature of the second model, and increases in their frequency were predictors of progression. The frequency of PI16+ fibroblasts was the second most important feature, and increases in their frequency were associated with stable skin fibrosis (Fig 7E, F). This finding suggests an active differentiation through the trajectory starting from PI16+ FBs and ending at COL8A1+ FBs during the early stages of progression of skin fibrosis. These findings highlight that incorporation of spatial information can improve the prediction of skin fibrosis compared to analysing changes in cell frequencies alone.

DISCUSSION

We present herein a novel approach for identification and functional characterisation of cell populations based on

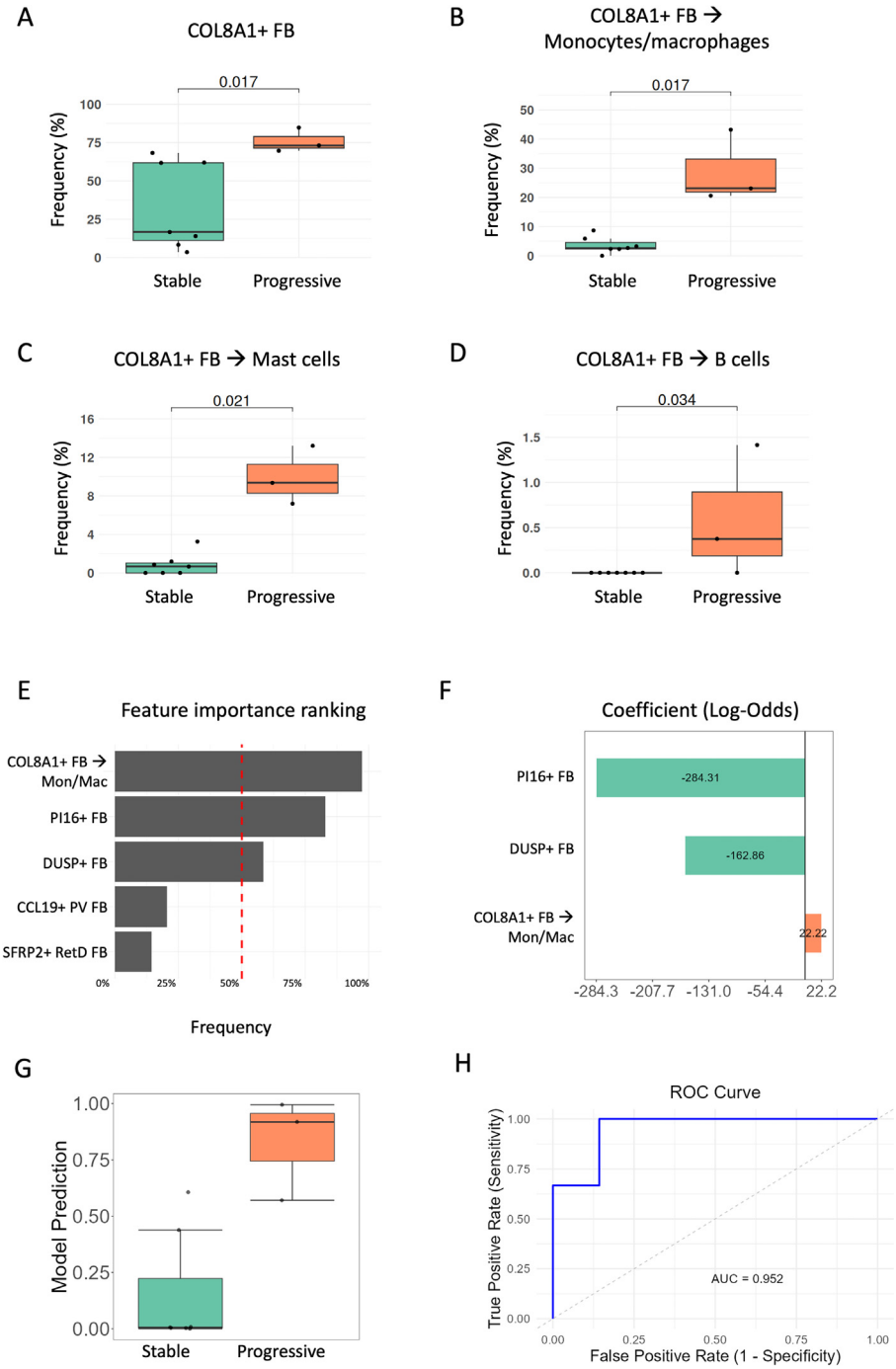

Figure 7. Predictors of progression of skin fibrosis in SSc. A-D, Frequencies of all COL8A1 + FBs (A) and of COL8A1 + FBs in spatial proximity to monocytes/macrophages (B), mast cells (C) or B cells (D) among all dermal cells. E, Top highly ranked features predictive of progression of skin fibrosis after bootstrapping with LASSO regression, starting from the frequencies of COL8A1 + FBs in spatial proximity to monocytes/macrophages, mast cells, or B cells, along with the frequencies of SFRP2 + RetD FBs, PI16 + FBs, DUSP + FBs, and CCL19 + PV FBs as predictors. (F) Increased frequencies of COL8A1 + fibroblasts in close spatial proximity to monocytes/macrophages were associated with a higher likelihood of progressive skin fibrosis, whereas elevated frequencies of PI16 + FBs and DUSP + FBs were linked to a decreased likelihood of fibrosis progression. (G) Model prediction results for each donor. (H) ROC curve and its AUC for evaluation of model performance. AUC, area under the curve; FB, fibroblasts; LASSO, least absolute shrinkage and selection operator; RetD, reticular dermis; ROC, receiver operating characteristic.

transcriptional profiles as well as on spatial localisation using cISH as an emerging technique, in conjunction with novel bioinformatical pipelines. We demonstrate the validity of this approach by confirming deregulation of previously identified subpopulations of fibroblasts [6,7,9]. Moreover, we complement the cISH-based approach with analysis of a spatial transcriptomics dataset from a second cohort of SSc patients and controls and with integration with publicly available scRNA-seq datasets from further SSc cohorts to combine the strengths of these different approaches.

Analyses of our cISH data using the BANKSY algorithm, which considers expression levels as well as spatial information, enabled us to identify 9 different fibroblast subpopulations in SSc and control skin. Our spatial phenotyping approach segregated SFRP2 + FBs and CCL19 + FBs into 4 distinct populations. We validated the distinct spatial localisation of these populations using 2 complementary methods, i.e. by spot deconvolution of the Visium dataset and by the neighbourhood analysis.

Of note, these spatially separated fibroblast populations do not only show differences in spatial localisation but are also functionally distinct. First, the spatially resolved fibroblast populations show differences in the expression levels of fibrosis-relevant genes and enrichment of distinct functional terms. For example, in SFRP2 + PapD FBs, the regulation of haemostasis was specifically enriched. However, in SFRP2 + RetD FBs, the response to mechanical stimulus was specifically enriched, and TGFβ signalling was stronger than that noted in SFRP2 + PapD FBs. The 2 populations of CCL19 + FBs also showed profound differences in the enrichment of functional terms relevant to fibrotic remodelling. Second, these pairs of fibroblasts segregated by spatially informed phenotyping differed with regards

to cellular interactions. SFRP2+ RetD FBs interacted with a wide range of immune cells. On the other hand, only a small proportion of dendritic cells were found in the surroundings of SFRP2+ PapD FBs. Third, these populations also displayed clear differences in ligand–receptor interactions. For example, ECM sensing by CD44 was specifically decreased in SFRP2+ RetD in SSc; furthermore, only CCL19+ nonPV FBs, but not CCL19+ PV FBs, signalled to NK cells via CXCL12–ACKR3. Fourth, the developmental trajectory differs for SFRP2+ PapD FBs and SFRP2+ RetD FBs, as these populations were located on 2 distinct trajectories. Fifth, these populations also show specific alterations in SSc skin. Together, these findings highlight that the novel, spatially defined populations of SFRP2+ RetD and SFRP2+ PapD FBs as well as CCL19+ PV and CCL19+ nonPV FBs are functionally clearly distinct with unique roles in the pathogenesis of SSc.

Our study also provides clear evidence that the profibrotic phenotype of fibroblasts in SSc is the result of the combined effects of different processes: (1) Our study demonstrates changes in the frequencies of fibroblast populations with increased frequencies in profibrotic populations. These changes include the elevated abundance of SFRP2+ RetD FB, which had demonstrated the highest collagen expression in our dataset. Shift towards profibrotic subsets have also been reported in non-spatially resolved scRNA-seq studies in SSc [6–9,22]. The changes in frequencies might be partially caused by a shift in the differentiation trajectory of precursor fibroblasts, particularly PI16+ FB, towards profibrotic subsets. (2) In addition, several individual populations are further biased towards a more profibrotic phenotype in SSc skin with upregulation of profibrotic genes and pathways, including TGFβ, Wingless/Int-1 (WNT), and ECM-modulating pathways. (3) The local neighbourhoods change drastically in SSc, thereby providing a microenvironment that fosters development of profibrotic fibroblasts. We detected upregulation of immune cell subsets with potential profibrotic roles such as monocytes/macrophages, mast cells, or plasma cells in the CCL19+ nonPV, COL8, and SFRP2 CNs in SSc. These changes in the interactions with immune cells are not a simple reflection of increased leukocyte counts in SSc skin, as the mentioned interactions are specific for certain leukocyte subsets and occur only with certain fibroblast populations. In contrast, other fibroblast subsets such as CCL19+ PV FBs demonstrate decreased interactions with immune cells in SSc.

We also provide first evidence that the frequencies of 2 fibroblast populations and their interactions with immune cells may help to predict the future course of skin fibrosis. The frequencies of COL8A1+ FBs were associated with future progression of skin fibrosis, whereas PI16+ FBs were associated with stable disease. This correlates well with the functional role of these 2 fibroblast subpopulations and their developmental trajectory. COL8A1+ FBs demonstrate enrichment in numerous pathways related to both fibrosis and inflammation. COL8A1+ FBs are also the end stage of differentiation of PI16+ FBs through a trajectory that involved SFRP2+ RetD FBs, another population with altered frequencies in SSc. This suggests that the active differentiation of PI16+ FBs towards COL8A1+ FBs, with potential recruitment of immune cells by COL8A1+ FBs, might drive progression of skin fibrosis. In line with this, the frequency of COL8A1+ FBs interacting with monocytes/macrophages provided an improved predictive power compared to the frequencies of all COL8A1+ FBs alone. Thus, by providing spatial information, our approach could provide an improved risk stratification than that based on evaluation of cell frequencies alone.

Our study has limitations. Although the SSc and control samples were matched for sex and age, the SSc biopsies were taken from the forearm, whereas the control samples were in part obtained from other locations such as the trunk and the lower extremities. Although our study provides extensive *in silico* validation of our findings, further experimental validation remains to be performed in follow-up studies. These might, for example, aim at confirming our findings at protein level by integration of our data with spatially resolved multiplexed protein data in SSc skin [23,24] or further functional studies on isolated subpopulations *in vitro*. The clinical relevance of our findings should be confirmed by performing cISH-based phenotyping on a higher number of SSc samples stratified by progression of skin fibrosis.

In summary, we used cISH in conjunction with novel bioinformatical pipelines that consider spatial context to identify 4 novel fibroblast subpopulations and to study the microenvironment and cellular interactions of fibroblasts in SSc and normal skin. We characterise SFRP2+ RetD FBs as s prototypical profibrotic, ECM-producing population that resides within a specific inflammatory niche, CCL19+ nonPV FBs as a proinflammatory population that attracts and activates immune cells, and COL8A1+ FBs as a population with roles in both ECM remodelling as well as immune cell recruitment that is associated with progression of skin fibrosis. These results may provide a rationale for specific therapeutic targeting of SFRP2+ RetD-, CCL19+ nonPV-, and COL8A1+ fibroblasts as disease-promoting fibroblast subsets and may stimulate follow-up studies to confirm the potential of COL8A1+ FB counts as a marker for fibrosis progression.

Competing interests

AHG received lecture fees from Boehringer Ingelheim. JHWD has consultancy relationships with Active Biotech, Anamar, ARXX, AstraZeneca, Bayer Pharma, Boehringer Ingelheim, Callidatas, Celgene, Galapagos, GSK, Inventiva, Janssen, Kyverna, Novartis, Pfizer, Quell Therapeutics and UCB; has received research funding from Anamar, ARXX, BMS, Bayer Pharma, Boehringer Ingelheim, Cantargia, Celgene, CSL Behring, Exo Therapeutics, Galapagos, GSK, Incyte, Inventiva, Kiniksa, Kyverna, Lassen Therapeutics, Mestag, Sanofi-Aventis, RedX, UCB and ZenasBio; and is CEO of 4D Science and scientific lead of FibroCure.

Acknowledgements

We thank Christoph Liebel, Philipp Steinbrecher, and Lukas Sokolowski for excellent technical assistance. We thank Michael Bailey, Trieu My Van, and Michael Leon from NanoString Technologies (now Bruker Spatial Biology) for supporting the CosMx runs.

Contributors

YNL, JHWD, and AEM designed the study. YNL, TF, AHG, ML, VD, AM, HC, and AEM were involved in acquisition and analysis of data. YNL, TF, AHG, ML, CB, ANP, TK, JH, AK, GS, SD, JHWD, and AEM were involved in interpretation of data. ML, CB, ACP, TK, JH, AK, and GS provided essential samples. All authors were involved in manuscript preparation and proofreading.

Funding

The project was supported by the following grants: Grants DI 1537/17-1, DI 1537/20-1, DI 1537/22-1, and DI 1537/23-1 of

the German Research Foundation; an unrestricted research grant from the Hiller Foundation (JHWD); MA 9219/2-1 of the German Research Foundation (AEM); a grant funded by the Deutsche Forschungsgemeinschaft (DFG, German Research Foundation) - 493659010 (AEM); grants 2021_EKEA.03 (AEM) and 2022_EKMS.02 (AEM) of the Else-Kröner-Fresenius-Foundation; The Edith Busch and World Scleroderma Foundation Research Grant Programme 2022-2023 (AEM); and the Research Committee of the Medical Faculty of the Heinrich-Heine University Düsseldorf (Forschungskommission; ID 2022-18, ID 2023-33, and ID 2023-31 to AHG, AEM, and JHWD, respectively).

Our analysis was supported by a de.NBI Cloud project (YNL) within the German Network for Bioinformatics Infrastructure (de.NBI) and ELIXIR-DE (Forschungszentrum Jülich and W-de.NBI-001, W-de.NBI-004, W-de.NBI-008, W-de.NBI-010, W-de.NBI-013, W-de.NBI-014, W-de.NBI-016, and W-de.NBI-022).

Patient consent for publication

All patients and control donors included in this study signed an informed concent, which has been reviewed by the local ethics committee.

Ethics approval

This stuty is approved by the ethics committee of the Medical Faculty of Heinrich Heine University Düsseldorf.

Provenance and peer review

Not comissioned; externally peer reviewed.

Supplementary materials

Supplementary material associated with this article can be found in the online version at doi:10.1016/j.ard.2025.06.002.

Orcid

Yi-Nan Li: http://orcid.org/0000-0001-8934-9361
Alexandru Micu: http://orcid.org/0000-0002-0154-1760
Ann-Christin Pecher: http://orcid.org/0000-0003-0201-0686
Jörg Henes: http://orcid.org/0000-0002-8385-6861
Pia Moinzadeh: http://orcid.org/0000-0002-8784-8615
Suzan Al-Gburi: http://orcid.org/0000-0002-1104-4784
Thomas Krieg: http://orcid.org/0000-0001-5616-8476
Alexander Kreuter: http://orcid.org/0000-0003-2275-499X
Jörg H.W. Distler: http://orcid.org/0000-0001-7408-9333
Alexandru-Emil Matei: http://orcid.org/0000-0003-1248-3145

REFERENCES

[1] Gabrielli A, Avvedimento EV, Scleroderma Krieg T. N Engl J Med 2009;360(19):1989–2003.
[2] Distler JHW, Györfi AH, Ramanujam M, Whitfield ML, Königshoff M, Lafyatis R. Shared and distinct mechanisms of fibrosis. Nat Rev Rheumatol 2019;15(12):705–30.
[3] Hinz B, Lagares D. Evasion of apoptosis by myofibroblasts: a hallmark of fibrotic diseases. Nat Rev Rheumatol 2020;16(1):11–31.
[4] Garrett SM, Baker Frost D, Feghali-Bostwick C. The mighty fibroblast and its utility in scleroderma research. J Scleroderma Relat Disord 2017;2(2):69–134.
[5] Györfi AH, Matei AE, Distler JHW. Targeting TGF-beta signaling for the treatment of fibrosis. Matrix Biol 2018;68-69:8–27.
[6] Zhu H, Luo H, Skaug B, Tabib T, Li YN, Tao Y, et al. Fibroblast subpopulations in systemic sclerosis: functional implications of individual subpopulations and correlations with clinical features. J Invest Dermatol 2024;144(6) 1251-61.e13.
[7] Ma F, Tsou PS, Gharaee-Kermani M, Plazyo O, Xing X, Kirma J, et al. Systems-based identification of the Hippo pathway for promoting fibrotic mesenchymal differentiation in systemic sclerosis. Nat Commun 2024;15(1):210.
[8] Gur C, Wang SY, Sheban F, Zada M, Li B, Kharouf F, et al. LGR5 expressing skin fibroblasts define a major cellular hub perturbed in scleroderma. Cell 2022;185(8) 1373-88.e20.
[9] Tabib T, Huang M, Morse N, Papazoglou A, Behera R, Jia M, et al. Myofibroblast transcriptome indicates $SFRP2^{hi}$ fibroblast progenitors in systemic sclerosis skin. Nat Commun 2021;12(1):4384.
[10] Windhager J, Zanotelli VRT, Schulz D, Meyer L, Daniel M, Bodenmiller B, et al. An end-to-end workflow for multiplexed image processing and analysis. Nat Protoc 2023;18(11):3565–613.
[11] Singhal V, Chou N, Lee J, Yue Y, Liu J, Chock WK, et al. BANKSY unifies cell typing and tissue domain segmentation for scalable spatial omics data analysis. Nat Genet 2024;56(3):431–41.
[12] Trapnell C, Cacchiarelli D, Grimsby J, Pokharel P, Li S, Morse M, et al. The dynamics and regulators of cell fate decisions are revealed by pseudotemporal ordering of single cells. Nat Biotechnol 2014;32(4):381–6.
[13] Buechler MB, Pradhan RN, Krishnamurty AT, Cox C, Calviello AK, Wang AW, et al. Cross-tissue organization of the fibroblast lineage. Nature 2021;593(7860):575–9.
[14] Merrick D, Sakers A, Irgebay Z, Okada C, Calvert C, Morley MP, et al. Identification of a mesenchymal progenitor cell hierarchy in adipose tissue. Science 2019;364(6438):eaav2501.
[15] Correa-Gallegos D, Ye H, Dasgupta B, Sardogan A, Kadri S, Kandi R, et al. $CD201^{+}$ fascia progenitors choreograph injury repair. Nature 2023;623(7988):792–802.
[16] Naba A, Clauser KR, Hoersch S, Liu H, Carr SA, Hynes RO. The matrisome: in silico definition and in vivo characterization by proteomics of normal and tumor extracellular matrices. Mol Cell Proteomics 2012;11(4) M111.014647.
[17] Schubert M, Klinger B, Klünemann M, Sieber A, Uhlitz F, Sauer S, et al. Perturbation-response genes reveal signaling footprints in cancer gene expression. Nat Commun 2018;9(1):20.
[18] Vahid MR, Brown EL, Steen CB, Zhang W, Jeon HS, Kang M, et al. High-resolution alignment of single-cell and spatial transcriptomes with CytoSPACE. Nat Biotechnol 2023;41(11):1543–8.
[19] Badia-I-Mompel P, Vélez Santiago J, Braunger J, Geiss C, Dimitrov D, Müller-Dott S, et al. decoupleR: ensemble of computational methods to infer biological activities from omics data. Bioinform Adv 2022;2(1):vbac016.
[20] Jin S, Plikus MV, Nie Q. CellChat for systematic analysis of cell-cell communication from single-cell transcriptomics. Nat Protoc 2025;20(1):180–219.
[21] Govindaraju P, Todd L, Shetye S, Monslow J, Puré E. CD44-dependent inflammation, fibrogenesis, and collagenolysis regulates extracellular matrix remodeling and tensile strength during cutaneous wound healing. Matrix Biol 2019;75-76:314–30.
[22] Valenzi E, Bulik M, Tabib T, Morse C, Sembrat J, Trejo Bittar H, et al. Single-cell analysis reveals fibroblast heterogeneity and myofibroblasts in systemic sclerosis-associated interstitial lung disease. Ann Rheum Dis 2019;78(10):1379–87.
[23] Rius Rigau A, Liang M, Devakumar V, Neelagar R, Matei AE, Györfi AH, et al. Imaging mass cytometry-based characterisation of fibroblast subsets and their cellular niches in systemic sclerosis. Ann Rheum Dis 2024.
[24] Rius Rigau A, Li YN, Matei AE, Györfi AH, Bruch PM, Koziel S, et al. Characterization of vascular niche in systemic sclerosis by spatial proteomics. Circ Res 2024;134(7):875–91.